Pattern Recognition 43 (2010) 1199–1206

Contents lists available at ScienceDirect

Pattern Recognition

journal homepage: www.elsevier.com/locate/pr

Active contours driven by local image fitting energy

Kaihua Zhang [a], Huihui Song [b], Lei Zhang [a,*]

[a] Department of Computing, The Hong Kong Polytechnic University, Hong Kong, China
[b] Department of Electronic Engineering and Information Science, University of Science and Technology of China, Hefei 230027, People's Republic of China

ARTICLE INFO

Article history:
Received 17 September 2009
Accepted 16 October 2009

Keywords:
Image segmentation
Chan–Vese (C–V) model
Active contour models
LBF model

ABSTRACT

A new region-based active contour model that embeds the image local information is proposed in this paper. By introducing the local image fitting (LIF) energy to extract the local image information, our model is able to segment images with intensity inhomogeneities. Moreover, a novel method based on Gaussian filtering for variational level set is proposed to regularize the level set function. It can not only ensure the smoothness of the level set function, but also eliminate the requirement of re-initialization, which is very computationally expensive. Experiments show that the proposed method achieves similar results to the LBF (local binary fitting) energy model but it is much more computationally efficient. In addition, our approach maintains the sub-pixel accuracy and boundary regularization properties.

1. Introduction

The active contour models (ACM) [1], which are based on the theory of surface evolution and geometric flows, have been extensively studied and successfully used in image processing. The level set method proposed by Osher and Sethian [2] is widely used in solving the problems of surface evolution. Later, geometric flows were unified into the classic energy minimization formulations for image segmentation [3–5,9–11,16,17,23]. Generally speaking, the existing ACM methods can be classified into two types: edge-based models [1–4,6,9,14,19,20,23] and region-based models [5,7,8,10,11,16–18,21]. Each of them has its own pros and cons.

The edge-based models utilize image gradient as an additional constraint to stop the contours on the boundaries of desired objects. Usually, a stopping function is used to attract the contours to the desired boundaries. In order to enlarge the capture range of the force, a balloon force term is often incorporated into the evolution function, which controls the contour to shrink or expand. However, it is difficult to choose a proper balloon force. Either a too large or too small balloon force will result in undesirable effects [10].

Region-based models utilize the image statistical information to construct constraints, and have more advantages over edge-based models. First, they do not use the image gradient, and can successfully segment objects with weak boundaries or even without boundaries. Second, the initial contour can start anywhere in the image, and the interior contours can be automatically detected. One of the most popular region-based models is the C–V model [5], which has been successfully used in binary phase segmentation with the assumption that each image region is statistically homogeneous. However, the C–V model does not work well for the images with intensity inhomogeneity. Vese and Chan extended their work in [17] to utilize multiphase level set functions to represent multiple regions. These models are called the piecewise constant (PC) models. Nonetheless, both the C–V and the PC models have the drawback described above.

In order to segment images with intensity inhomogeneities, Vese and Chan [17] and Tsai et al. [16] proposed two similar models, which are called piecewise smooth (PS) model. However, these methods are computationally inefficient. More discussions above the properties of PC model and PS model can be found in [10,11]. Li et al. [10,11] proposed the LBF (local binary fitting) model, which utilizes the local image information as constraints, can well segment objects with intensity inhomogeneities. Furthermore, LBF model has better performance than PC and PS models in segmentation accuracy and computational efficiency.

In this paper, we propose a novel ACM model that can be used to segment images with intensity inhomogeneities. We utilize the local image information to construct a local image fitting (LIF) energy functional, which can be viewed as a constraint of the differences between the fitting image [10,11] and the original image. Furthermore, a novel method is used to regularize the level set function by using Gaussian kernel filtering after each iteration. In addition, re-initialization is not needed in the proposed method. The complexity analysis and experimental results show that the proposed method is more efficient than the LBF model, while yielding similar results.

The rest of the paper is organized as follows. In Section 2, we review some classic models and indicate their limitations. Section 3 describes our model and its variational formulation. In Section 4,

* Corresponding author. Tel.: +852 27667355.
E-mail addresses: zhkhua@mail.ustc.edu.cn (K. Zhang), freebird@mail.ustc.edu.cn (H. Song), cslzhang@comp.polyu.edu.hk (L. Zhang).

0031-3203/$ - see front matter © 2009 Elsevier Ltd. All rights reserved.
doi:10.1016/j.patcog.2009.10.010

we validate our method by various experimentations on synthetic and real images. Conclusion is made in Section 5.

2. Background

2.1. The Mumford and Shah (MS) model

In [8], Mumford and Shah formulated the image segmentation problem as follows: find an optimal piecewise smooth approximation function u of image I, which varies smoothly within each sub-region Ω_i of image domain $\Omega \subset R^2$, and rapidly or discontinuously goes across the boundaries of Ω_i. They proposed the following energy functional:

$$E^{\mathrm{MS}}(u,C)=\int_{\Omega}(u-I)^2\,\mathrm{d}x+\mu\int_{\Omega/C}|\nabla u|^2\,\mathrm{d}x+\nu|C|,\quad x\in\Omega \tag{1}$$

where $|C|$ is the length of the contour C, $\mu,\nu\geq 0$ are fixed parameters.

The unknown set C and the non-convexity of the above energy functional make it difficult to be minimized. Some alternative methods have been proposed to simplify or modify the above functional, including the two popular ones introduced as follows.

2.2. The C–V model

Chan and Vese [5] proposed an ACM based on the Mumford–Shah model [8]. Let $I:\Omega\to R$ be an input image and C be a closed curve, the energy functional is defined by

$$\begin{aligned}E^{\mathrm{CV}}(C,c_1,c_2)&=\mu\cdot\mathrm{length}(C)+\nu\cdot\mathrm{area}(\mathrm{inside}(C))\\&\quad+\lambda_1\int_{\mathrm{inside}(C)}|I-c_1|^2\,\mathrm{d}x+\lambda_2\int_{\mathrm{outside}(C)}|I-c_2|^2\,\mathrm{d}x,\quad x\in\Omega\end{aligned} \tag{2}$$

where $\mu\geq 0$, $\nu\geq 0$, $\lambda_1,\lambda_2>0$ are fixed parameters. The Euclidean length term is used to regularize the contour. c_1 and c_2 are two constants that approximate the image intensities inside and outside the contour C, respectively.

Minimizing the above energy functional by using the steepest descent method [22], and representing the contour C with zero level set, i.e. $C=\{x\in\Omega|\phi(x)=0\}$, we obtain the following variational formulation:

$$\begin{cases}c_1(\phi)=\dfrac{\int_{\Omega}IH(\phi)\,\mathrm{d}\Omega}{\int_{\Omega}H(\phi)\,\mathrm{d}\Omega},\quad c_2(\phi)=\dfrac{\int_{\Omega}I(1-H(\phi))\,\mathrm{d}\Omega}{\int_{\Omega}(1-H(\phi))\,\mathrm{d}\Omega}\\ \dfrac{\partial\phi}{\partial t}=\delta(\phi)\left[\mu\,\mathrm{div}\left(\dfrac{\nabla\phi}{|\nabla\phi|}\right)-\nu-\lambda_1(I-c_1)^2+\lambda_2(I-c_2)^2\right]\end{cases} \tag{3}$$

The data fitting term $-\lambda_1(I-c_1)^2+\lambda_2(I-c_2)^2$ plays a key role in curve evolution, and λ_1 and λ_2 govern the tradeoff between the first term and the second term. In most cases, we set $\lambda_1=\lambda_2$ and $\nu=0$. μ is a scaling parameter. If it is small enough, then small objects are likely to be extracted; if it is large, big objects can be detected [5].

Obviously, in Eq. (3), c_1 and c_2 are related to the global properties of the image contents inside and outside the contour, respectively. However, such global image information is not accurate if the image intensity inside or outside the contour is inhomogeneous.

2.3. The piecewise smooth (PS) model

For the images with intensity inhomogeneities, the C–V model does not work well. In order to overcome this difficulty, in [17] Vese and Chan proposed another method which aims at expressing the intensities inside and outside the contour as piecewise smooth functions instead of constants. The following energy functional was defined:

$$\begin{aligned}E^{\mathrm{PS}}(u^+,u^-,\phi)&=\int_{\Omega}|u^+-I|^2H(\phi)\,\mathrm{d}x+\int_{\Omega}|u^--I|^2(1-H(\phi))\,\mathrm{d}x\\&\quad+\mu\int_{\Omega}|\nabla u^+|^2H(\phi)\,\mathrm{d}x+\mu\int_{\Omega}|\nabla u^-|^2(1-H(\phi))\,\mathrm{d}x\\&\quad+\nu\int_{\Omega}|\nabla H(\phi)|,\quad x\in\Omega\end{aligned} \tag{4}$$

where $\mu,\nu\geq 0$ are fixed parameters, $I:\Omega\to R$ denotes the original image, $u^+(x)$ and $u^-(x)$ are smooth functions in the sub-regions $\Omega^+=\{x\in\Omega:\phi(x)>0\}$ and $\Omega^-=\{x\in\Omega:\phi(x)<0\}$, respectively.

Minimizing the above energy functional, we get the following Euler–Lagrange equations:

$$u^+-I=\mu\Delta u^+\ \text{in}\ \{x\in\Omega:\phi(x;t)>0\}$$

$$\frac{\partial u^+}{\partial\vec{n}}=0\quad\text{on}\ \{x\in\Omega:\phi(x;t)=0\}\cup\partial\Omega$$

$$u^--I=\mu\Delta u^-\ \text{in}\ \{x\in\Omega:\phi(x;t)<0\}$$

$$\frac{\partial u^-}{\partial\vec{n}}=0\quad\text{on}\ \{x\in\Omega:\phi(x;t)=0\}\cup\partial\Omega$$

$$\frac{\partial\phi}{\partial t}=\delta(\phi)\left[\nu\,\mathrm{div}\left(\frac{\nabla\phi}{|\nabla\phi|}\right)-|u^+-I|^2-\mu|\nabla u^+|^2+|u^--I|^2+\mu|\nabla u^-|^2\right] \tag{5}$$

Obviously, u^+ and u^- must be obtained by solving the two partial differential equations (PDEs) before each iteration, and the computational cost is very expensive. Moreover, in the implementation of PS model, u^+ and u^- must be extended to the whole image domain, which is difficult to implement and also increases the computational cost. In summary, the high complexity limits the application of PS model in practice.

2.4. The LBF model

Li et al. [10,11] proposed the LBF model by embedding the local image information. LBF is able to segment images with intensity inhomogeneities and is much more efficient and accurate than the PS model. The basic idea is to introduce a kernel function to define an LBF energy functional as follows:

$$\begin{aligned}E^{\mathrm{LBF}}(C,f_1,f_2)&=\lambda_1\int_{\Omega}\int_{\mathrm{inside}(C)}K_\sigma(x-y)|I(y)-f_1(x)|^2\,\mathrm{d}y\,\mathrm{d}x\\&\quad+\lambda_2\int_{\Omega}\int_{\mathrm{outside}(C)}K_\sigma(x-y)|I(y)-f_2(x)|^2\,\mathrm{d}y\,\mathrm{d}x,\quad x,y\in\Omega\end{aligned} \tag{6}$$

where $\lambda_1,\ \lambda_2>0$ are fixed parameters, $I:\Omega\to R$ is an input image, K_σ is a Gaussian kernel with standard deviation σ, f_1 and f_2 are two smooth functions that approximate the local image intensities inside and outside the contour C, respectively.

In the level set method, $C\subset\Omega$ can be represented by the zero level set of a Lipschitz function $\phi:\Omega\subset R$. Minimizing the energy functional E^{LBF} with respect to ϕ, we have the gradient descent flow as follows:

$$\frac{\partial\phi}{\partial t}=-\delta_\varepsilon(\phi)(\lambda_1e_1-\lambda_2e_2) \tag{7}$$

In order for stable evolution of the level set function, a distance regularized term in [9] is incorporated into (7). Moreover, the Euclidean length term is used to regularize the zero contour of ϕ.

Finally, the total variational formulation is as follows:

$$\frac{\partial\phi}{\partial t}=\mu\left(\nabla^2\phi-\mathrm{div}\left(\frac{\nabla\phi}{|\nabla\phi|}\right)\right)+\nu\delta_\varepsilon(\phi)\mathrm{div}\left(\frac{\nabla\phi}{|\nabla\phi|}\right)-\delta_\varepsilon(\phi)(\lambda_1 e_1-\lambda_2 e_2), \tag{8}$$

the coefficients λ_1 and λ_2 weight the two integrals over regions inside and outside the contour. In most cases, we fix $\lambda_1=\lambda_2$. In Eq. (8), e_1 and e_2 are defined as follows:

$$\begin{cases} e_1(x)=\int_\Omega K_\sigma(y-x)|I(x)-f_1(y)|^2\,\mathrm{d}y \\ e_2(x)=\int_\Omega K_\sigma(y-x)|I(x)-f_2(y)|^2\,\mathrm{d}y \end{cases} \tag{9}$$

with

$$\begin{cases} f_1(x)=\dfrac{K_\sigma*[H_\varepsilon(\phi)I(x)]}{K_\sigma*H_\varepsilon(\phi)} \\ f_2(x)=\dfrac{K_\sigma*[(1-H_\varepsilon(\phi))I(x)]}{K_\sigma*(1-H_\varepsilon(\phi))} \end{cases} \tag{10}$$

The standard deviation σ of the kernel plays an import role in practical applications. σ can be seen as a scale parameter that controls the region-scalability from small neighborhood to the whole image domain [11]. The scale parameter should be properly chosen according to the images. A too small σ may cause undesirable result, while a too large σ will cause high computational cost.

In the above equations, the regularized versions of Heaviside function H and Dirac function δ are utilized as follows:

$$\begin{cases} H_\varepsilon(z)=\dfrac{1}{2}\left[1+\dfrac{2}{\pi}\arctan\left(\dfrac{z}{\varepsilon}\right)\right] \\ \delta_\varepsilon(z)=\dfrac{1}{\pi}\cdot\dfrac{\varepsilon}{\varepsilon^2+z^2}, \quad z\in R \end{cases} \tag{11}$$

The parameter ε affects the profile of $\delta_\varepsilon(\phi)$. A larger ε will lead to a broader profile, which will enlarge the capture range but decrease the accuracy in the final contour location.

Obviously, f_1 and f_2 of Eq. (10) can be viewed as the weighted averages of the image intensities in a Gaussian window inside and outside the contour, respectively. This is why the LBF model can well handle image with intensity inhomogeneity.

3. ACM with local image fitting (LIF)

3.1. LIF model and its variational level set formulation

A local fitted image (LFI) formulation is defined as follows:

$$I^{\mathrm{LFI}}=m_1H_\varepsilon(\phi)+m_2(1-H_\varepsilon(\phi)) \tag{12}$$

where m_1 and m_2 are defined as follows:

$$\begin{cases} m_1=\mathrm{mean}(I\in(\{x\in\Omega|\phi(x)<0\}\cap W_k(x))) \\ m_2=\mathrm{mean}(I\in(\{x\in\Omega|\phi(x)>0\}\cap W_k(x))) \end{cases} \tag{13}$$

where $W_k(x)$ is a rectangular window function, e.g. a truncated Gaussian window or a constant window. In our experiment, we choose a truncated Gaussian window $K_\sigma(x)$ with standard deviation σ and of size $4k+1$ by $4k+1$, where k is the greatest integer smaller than σ. Similar segmentation results can be achieved if we choose a constant window.

In this paper we propose a local image fitting energy functional by minimizing the difference between the fitted image and the original image. The formulation is as follows:

$$E^{\mathrm{LIF}}(\phi)=\frac{1}{2}\int_\Omega|I(x)-I^{\mathrm{LFI}}(x)|^2\,\mathrm{d}x, \quad x\in\Omega \tag{14}$$

Using the calculus of variation and the steepest descent method [22], we minimize $E^{\mathrm{LIF}}(\phi)$ with respect to ϕ to get the corresponding gradient descent flow (please refer to Appendix A for detailed derivation):

$$\frac{\partial\phi}{\partial t}=(I-I^{\mathrm{LFI}})(m_1-m_2)\delta_\varepsilon(\phi) \tag{15}$$

where $\delta_\varepsilon(\phi)$ is the regularized Dirac function defined in Eq. (11).

3.2. Implementation

In the traditional level set methods [2,15,20], in order to prevent the level set function ϕ from being too steep or flat, the level set function is initialized to be a signed distance function (SDF) to its interface, and during the evolution, re-initialization is necessary to reshape the degraded level set function as an SDF. Unfortunately, this is an expensive procedure. Li et al. [9] proposed a variational formulation penalizing the deviation of the level set function from an SDF, which is useful in the application of variational level set methods but cannot be applied to the pure partial differential equation (PDE) driven level set methods.

When the level set function ϕ is chosen as an SDF, it will satisfy $|\nabla\phi|=1$ [15]. As pointed out in [5,24], we can replace $\delta(\phi)$ by $|\nabla\phi|$ in order to enlarge the capture range. Thus the term $\mathrm{div}(\nabla\phi/|\nabla\phi|)\delta(\phi)$ used for smoothness regularization can be replaced by $\mathrm{div}(\nabla\phi/|\nabla\phi|)|\nabla\phi|$, which equals to the Laplacian of ϕ when ϕ is an SDF. As pointed out by Shi et al. [12], based on the scale-space theory [13], the evolution of a function according to its Laplacian is equivalent to Gaussian filtering the initial condition of the function. So the previous iteration result of the level set function can be viewed as the initial condition for the next iteration, i.e. $\phi^{n+1}=G_{\sqrt{\Delta t}}*\phi^n$, where $G_{\sqrt{\Delta t}}$ is a Gaussian kernel with variance Δt, and it can be viewed as the solution to the following equation at the time $t=(n+1)\Delta t$:

$$\phi_t=\Delta\phi \tag{16}$$

with the initial condition $\phi(x,t=n\Delta t)=\phi^n$, where n is the iteration number and Δt is the time-step.

To obtain the solution to Eq. (16), ϕ^{n+1} can also be expressed as the following iteration:

$$\phi^{n+1}=\phi^n+\Delta t\Delta\phi^n \tag{17}$$

where Δt is the time-step. Obviously, the solution we obtain from Eq. (17) is in general not smooth because the Laplacian term is defined on a point-by-point basis, whereas the Gaussian filtering uses all the points around the center point to make the level set function smooth.

As we use a Gaussian kernel to regularize the level set function, the traditional regularized term $\mathrm{div}(\nabla\phi/|\nabla\phi|)\delta(\phi)$ can be removed [6,12]. The main steps of the algorithm can be summarized as

1. Initialize the level set function ϕ to be a binary function as follows:
$$\phi(x,t=0)=\begin{cases} -\rho, & x\in\Omega_0-\partial\Omega_0 \\ 0, & x\in\partial\Omega_0 \\ \rho, & x\in\Omega-\Omega_0 \end{cases} \tag{18}$$
where $\rho>0$ is a constant, Ω_0 is a subset in the image domain Ω and $\partial\Omega_0$ is the boundary of Ω_0.
2. Evolve the level set function ϕ according to Eq. (15).
3. Regularize the level set function by a Gaussian kernel, i.e. $\phi=G_\varsigma*\phi$, where ς is the standard deviation, which should be larger than the square root of the time-step Δt in order to enhance the smoothing capacity.

4. Check whether the evolution is stationary. If not, return to step 2.

Generally speaking, in step 3 the standard deviation ς should be chosen between 0.45 and 1 according to our experiments. If the noise is high, a larger ς should be chosen. The size of the Gaussian kernel can be truncated as an $n \times n$ mask for efficiency, where n is typically < 6.

In the proposed method, the most time-consuming operation is in step 3 and the computational complexity is $O(n^2 \times N)$, where N is the image size. The computational complexity of re-initialization is $O(N \times N)$. Since $n^2 \ll N$, our method is much more computationally efficient than the traditional level set method.

3.3. Implementation without re-initialization

In order to compare our method with the variational level set formulation without re-initialization proposed by Li et al. [9], we give another implementation. The Euclidean length term that regularizes the level set function is incorporated into this formulation, and the total variational level set formulation is as follows:

$$\frac{\partial \phi}{\partial t} = \mu\left(\nabla^2\phi - \mathrm{div}\left(\frac{\nabla\phi}{|\nabla\phi|}\right)\right) + \nu\delta_\varepsilon(\phi)\mathrm{div}\left(\frac{\nabla\phi}{|\nabla\phi|}\right) + (I - I^{\mathrm{LFI}})(m_1 - m_2)\delta_\varepsilon(\phi) \tag{19}$$

We implement this formulation by using the similar steps described in Section 3.2 except step 3. As we will see in Section 4.1, by this method the proposed energy functional is easy to be trapped into local minima, which result in unsatisfactory segmentation results.

3.4. Advantages over the LBF model

Although re-initialization is unnecessary in the implementation of LBF model, the computational complexity is still very high. Compared with our method, the main computational cost of LBF is spent on the term $\lambda_1 e_1 - \lambda_2 e_2$ in Eq. (8). Instead, we use a cost-effective method to compute it in this paper. Obviously, e_1 can be re-written as follows:

$$\begin{aligned} e_1(x) &= \int_\Omega K_\sigma(y-x)|I(x) - f_1(y)|^2\,\mathrm{d}y \\ &= I^2(x)[K_\sigma(x) * 1] - 2I(x)[K_\sigma(x) * f_1(x)] + K_\sigma(x) * f_1^2(x), \quad x \in \Omega \end{aligned}$$

and e_2 can be written as

$$\begin{aligned} e_2(x) &= \int_\Omega K_\sigma(y-x)|I(x) - f_2(y)|^2\,\mathrm{d}y \\ &= I^2(x)[K_\sigma(x) * 1] - 2I(x)[K_\sigma(x) * f_2(x)] + K_\sigma(x) * f_2^2(x), \quad x \in \Omega \end{aligned}$$

So

$$\begin{aligned} \lambda_1 e_1 - \lambda_2 e_2 = (\lambda_1 - \lambda_2)I^2(x)[K_\sigma(x) * 1] - 2I(x)[K_\sigma(x) * (\lambda_1 f_1 - \lambda_2 f_2)] \\ + K_\sigma(x) * (\lambda_1 f_1^2 - \lambda_2 f_2^2) \end{aligned} \tag{20}$$

The convolution term $K_\sigma(x) * 1$ can be computed only once before the iteration. However, the other two convolution terms must be computed in each iteration. In practice, we truncate K_σ as an $m \times m$ mask for efficiency, where m is the smallest odd number bigger than 4σ. The total computational complexity of LBF model is $O(m^2 \times N)$. In the implementation, the size of the regularized Gaussian kernel in our method is truncated into an $n \times n$ mask with $n \leq 5$. However, σ is often greater than 3 in our experiments, so $n^2 \ll m^2$ and our method is much more computationally efficient than the LBF model.

4. Experimental results

Our algorithm is implemented in Matlab 7.0 on a 2.8-GHz Intel Pentium IV personal computer. In this section, we apply our method to synthetic images and real images of different modalities, and use the same parameters $\rho = 1$, $\varepsilon = 1$, $\varsigma = 0.45$, $n = 3$ and time-step $\Delta t = 0.025$. Parameter σ is chosen by experience according to the images The Matlab source code of the proposed algorithm can be downloaded at http://www.comp.polyu.edu.hk/~cslzhang/code/LIF.zip.

4.1. Comparisons between the methods in Sections 3.2 and 3.3

We name the method described in Section 3.2 the Gaussian regularizing level set model (GRLSM), and name the method in

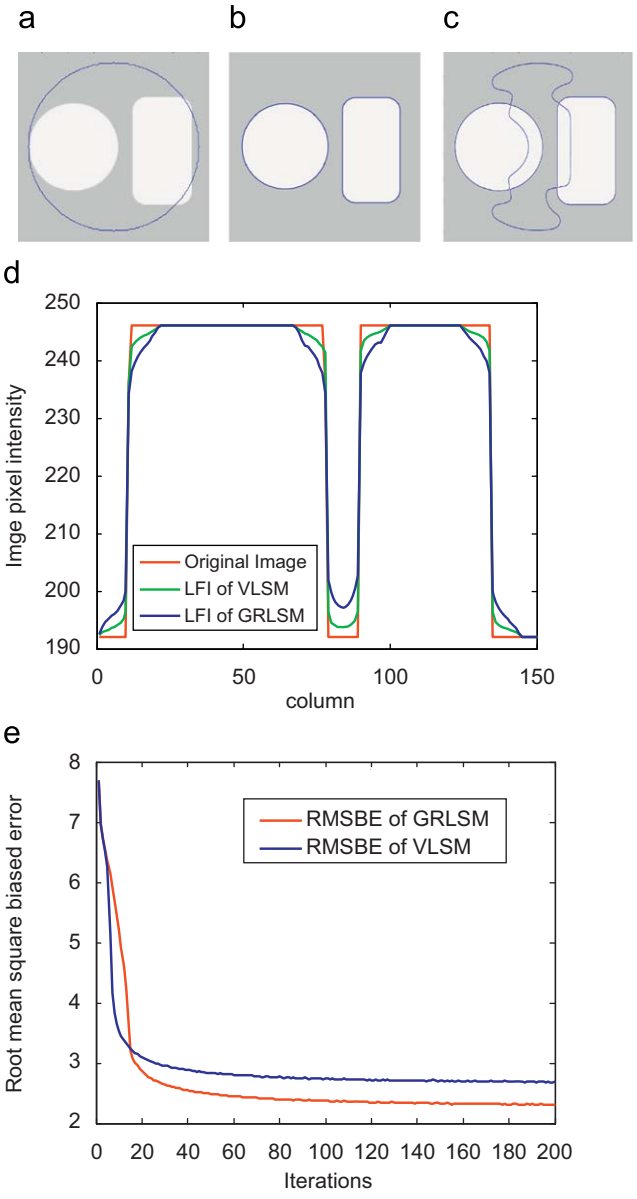

Fig. 1. Demonstrations of the globally optimal property of GRLSM and the locally optimal property of VLSM, respectively: (a) initial contour; (b) segmentation result of GRLSM; (c) segmentation result of VLSM; (d) cross-sections of the middle rows of the original image (the red solid line), the local fitted images (LFI) by VLSM (the green solid line) and GRLSM (the blue solid line); and (e) the RMSBE values of GRLSM (the red solid line) and VLSM (the blue solid line) during the evolution. The parameter σ=5. (For interpretation of the references to color in this figure legend, the reader is referred to the web version of this article.)

Section 3.3 the variational level set model (VLSM). We use the root mean square biased error (RMSBE) to evaluate the differences between the fitted image and the original image:

$$RMSBE = \sqrt{\frac{1}{N}\sum |I(x) - I^{\mathrm{LFI}}(x)|^2}, \quad x \in \Omega \tag{21}$$

where N is the size of the image.

Fig. 1 shows the segmentation results of GRLSM and VLSM on a synthetic image. We set $\sigma = 5$. Fig. 1(d) shows that the fitted images of the two methods are very similar and both of them can match the original image well. Fig. 1(e) shows that the RMSBE values of the two methods are almost the same during the evolution. However, Fig. 1(c) shows that the segmentation result is unsatisfactory by VLSM. The experiments in Section 4.2 also show that the results by VLSM are unsatisfactory in most cases. This is because the distance regularized term in Li et al.'s [9] method only satisfies the necessary condition of the SDF, but not the sufficient condition. If the distance regularized term in [9] is incorporated into Eq. (15), the model is easy to be trapped into the local minimum. The experimental results in Fig. 1 validate GRLSM can conveniently achieve satisfying results.

4.2. Comparisons with the C–V model and the LBF model

The experiment in Fig. 2 validates that our method can achieve sub-pixel segmentation accuracy. As can be seen from Fig. 2(c), with the C–V model the two middle fingers stick together, which is not desired. The segmentation result by our method is shown in Fig. 2(d), which achieves sub-pixel segmentation accuracy of the finger boundaries. The final contour accurately reflects the true hand shape.

Fig. 3 shows the segmentation results on a synthetic image with seven different intensities. Fig. 3(a) is the initial contour, (b) is the segmentation result of the synthetic image without noise. Obviously, these objects with different intensities are successfully extracted. We then added Gaussian noise to the clean image. The noisy image is shown in Fig. 3(c) and Fig. 3(d) shows the corresponding segmentation result of our method on the noisy

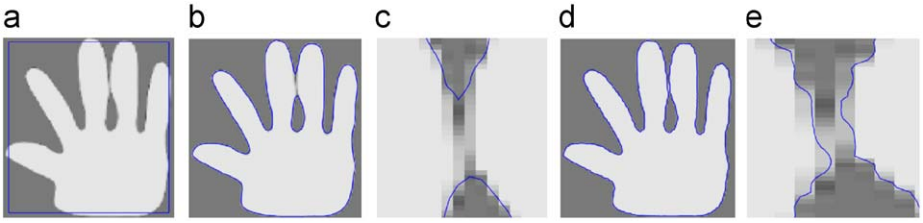

Fig. 2. Segmenting a hand phantom using the C–V model and the proposed method: (a) initial contour; (b) segmentation result by the C–V model; (c) zoomed view of the narrow parts in (b); (d) segmentation result by our method; and (e) zoomed view of the narrow parts in (d). The parameter σ=3 in this example.

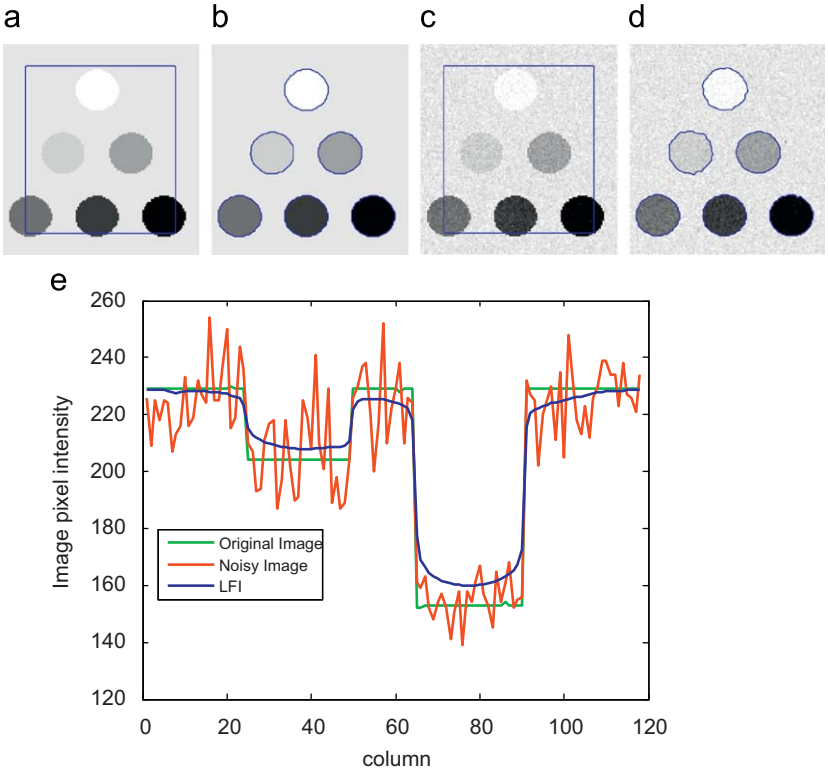

Fig. 3. Segmentation results on synthetic images with and without noise: (a) initial contour; (b) segmentation result of clean image; (c) initial contour; (d) segmentation result of noisy image; and (e) cross-sections of the middle rows of the original image (the green solid line), noisy image (the red solid line) and fitted image (the blue solid line). The parameter σ=3. (For interpretation of the references to color in this figure legend, the reader is referred to the web version of this article.)

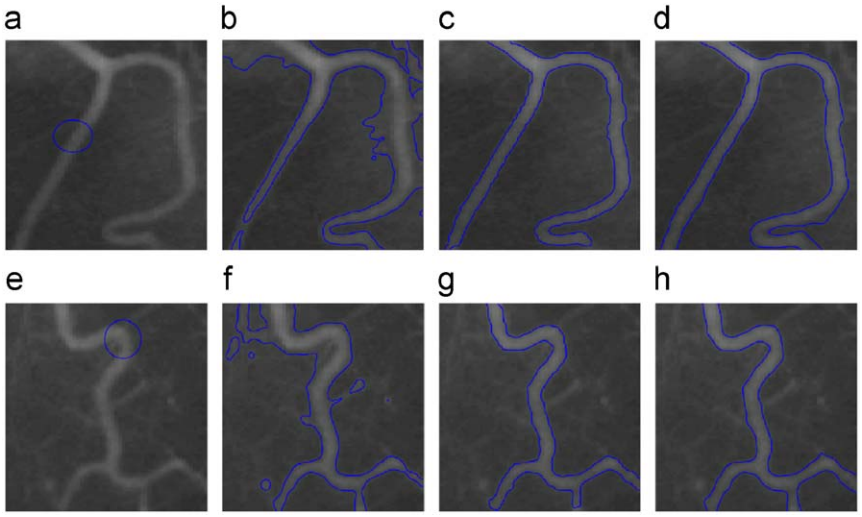

Fig. 4. Segmentation results on real blood vessel images: (a) and (e) are initial contours; (b) and (f) are the results by the C–V model; (c) and (g) are the results by the LBF model; (d) and (h) are the results by the proposed method. The parameter σ=3.

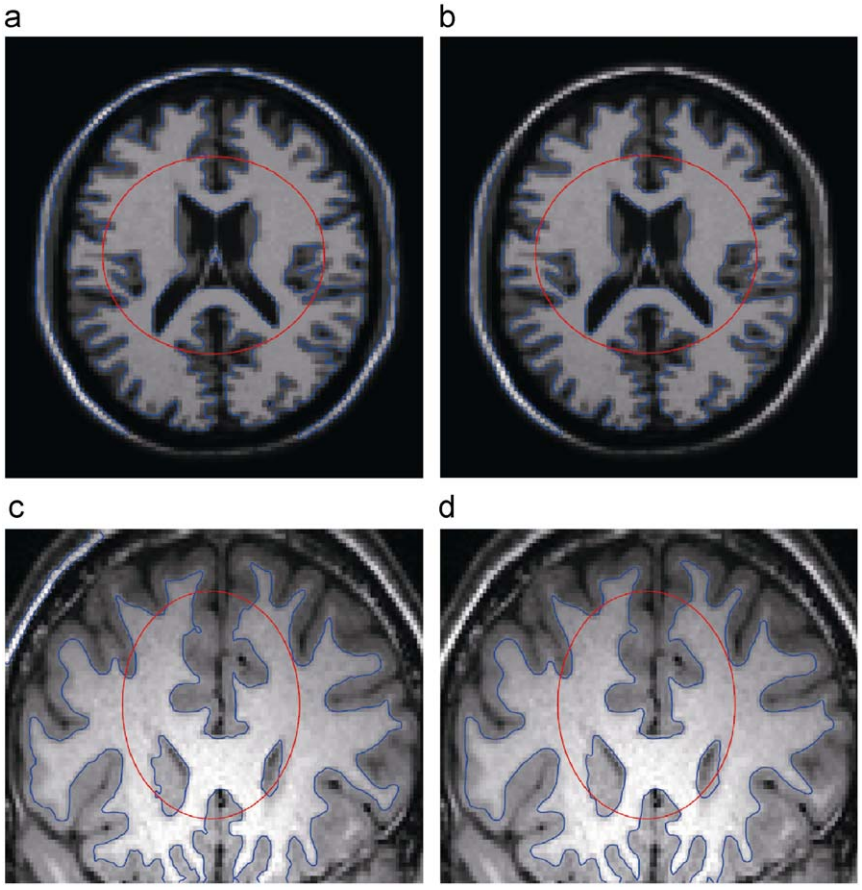

Fig. 5. Segmentation on brain MR images: (a) and (c) are the results by the LBF model; (b) and (d) are the results by our method. The red solid lines represent the initial contours. The parameter σ=10. (For interpretation of the references to color in this figure legend, the reader is referred to the web version of this article.)

image. We see that the corresponding segmentation result is similar to that of the synthetic image without noise in Fig. 3(b). Although the noise is relatively high as shown in Fig. 3(e), our method can well fit the original image, while reducing the noise significantly.

Fig. 4 compares the performance of the C–V model, the LBF model and our method in segmenting two real blood vessel X-ray images. We choose $\sigma = 3$. The vessel images are of intensity inhomogeneities. Figs. 4(b) and (f) show the results by C–V model. It can be observed that parts of the background and foreground are mixed together. Figs. 4(c) and (g) show that the LBF model achieves satisfying segmentation results. Figs. 4(d) and (h) show the results by our method, which are similar to the results by the LBF model.

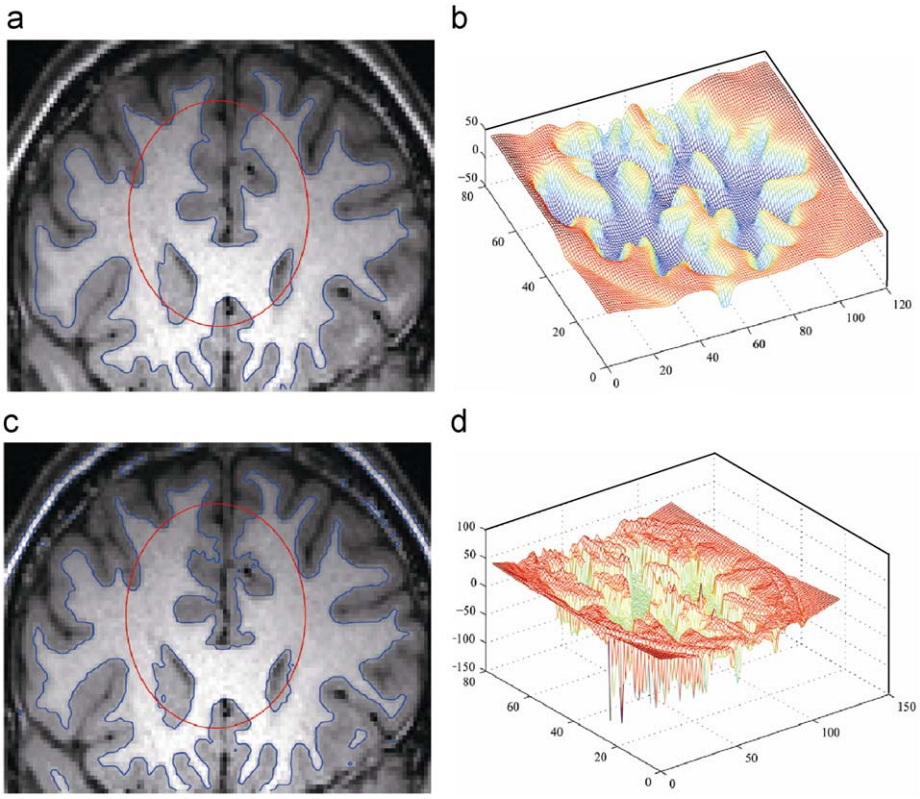

Fig. 6. Segmentation results by the level set function with and without regularization: (a) is the segmentation result by our method with regularization, and (b) is the corresponding final level set function. (c) shows the segmentation result without regularization, and (d) is the corresponding final level set function. The red solid lines represent the initial contours. (For interpretation of the references to color in this figure legend, the reader is referred to the web version of this article.)

Table 1
Iterations and CPU time (in seconds) by LIF model and LBF model.

	Fig. 4(a)		Fig. 4(e)		Fig. 5(a)		Fig. 5(c)	
	103×131 pixels		111×110 pixels		91×112 pixels		119×78 pixels	
	Iterations	Time (s)	Iterations	Time (s)	Iterations	Time (s)	Iterations	Time (s)
LIF	200	10.64	50	6.68	80	10.33	200	45.14
LBF	400	63.62	200	37.04	85	20.78	200	65.47

Fig. 5 shows the segmentation results on two brain MR images by LBF model and our method. We choose $\sigma = 10$. Again, our method achieves almost the same results as the LBF model. Fig. 6 demonstrates the results for the level set function with or without regularization for brain MR image. Fig. 6(a) shows the segmentation result by our method with regularization and Fig. 6(b) shows the corresponding final level set function. It can be seen that the final level set function is very smooth and this validates that the proposed level set method is capable of keeping the level set function regular. However, the final level set function without regularization has very large values around the zero level set (see Fig. 6(d)), resulting in very noisy arbitrary gradients, which cause the evolution to be unstable.

The converged iterations and CPU time for Figs. 4 and 5 are compared in Table 1. The sizes of the tested images are also listed. It can be observed that our method is much faster than LBF model in each iteration, and in most cases, the number of iterations by our method is fewer than that by LBF model. Thus the proposed method is more efficient.

5. Conclusions

In this paper, we proposed a novel active contour model driven by local image fitting (LIF) energy. The proposed LIF energy functional has less computational complexity than the local binary fitting (LBF) energy functional. A novel level set method based on Gaussian filtering was used to implement our variational formulation, and the experimental results revealed that it is not only robust to prevent the energy functional from being trapped into local minimum, but also capable of keeping the level set function regular. Experiments demonstrated that our method can achieve satisfying segmentation results as the LBF model but it is much more efficient. It should be pointed out that the proposed

Gaussian regularizing level set method (GRLSM) can be easily extended to pure PDE driven level set methods.

Appendix A. Derivation of the gradient descent flow

In Eq. (14), we add the variation η to the level set function ϕ such that $\tilde{\phi}=\phi+\varepsilon\eta$. Keeping m_1 and m_2 fixed, differentiating with respect to ϕ, and letting $\varepsilon\to 0$, we have

$$\begin{aligned}\frac{\delta E^{\mathrm{LIF}}(\phi)}{\delta\phi} &= \lim_{\varepsilon\to 0}\frac{d}{d\varepsilon}\left(\frac{1}{2}\int_{\Omega}|I-m_1H_\varepsilon(\tilde{\phi})-m_2(1-H_\varepsilon(\tilde{\phi}))|^2\,dx\right)\\ &= \lim_{\varepsilon\to 0}(-\int_{\Omega}[I-m_1H_\varepsilon(\tilde{\phi})-m_2(1-H_\varepsilon(\tilde{\phi}))](m_1-m_2)\delta_\varepsilon(\tilde{\phi})\eta\,dx)\\ &= -\int_{\Omega}[I-m_1H_\varepsilon(\phi)-m_2(1-H_\varepsilon(\phi))](m_1-m_2)\delta_\varepsilon(\phi)\eta\,dx\end{aligned}$$

So we obtain the Euler–Lagrange equation

$$-[I-m_1H_\varepsilon(\phi)-m_2(1-H_\varepsilon(\phi))](m_1-m_2)\delta_\varepsilon(\phi)=0$$

By the steepest gradient descent method [19], we get the following gradient descent flow:

$$\begin{aligned}\frac{\partial\phi}{\partial t} &= (I-m_1H_\varepsilon(\phi)-m_2(1-H_\varepsilon(\phi)))(m_1-m_2)\delta_\varepsilon(\phi)\\ &= (I-I^{\mathrm{LFI}})(m_1-m_2)\delta_\varepsilon(\phi)\end{aligned}$$

References

[1] M. Kass, A. Witkin, D. Terzopoulos, Snakes: active contour models, International Journal of Computer Vision 1 (1988) 321–331.

[2] S. Osher, J.A. Sethian, Fronts propagating with curvature dependent speed: algorithms based on Hamilton–Jacobi formulations, Journal of Computational Physics 79 (1988) 12–49.

[3] V. Caselles, R. Kimmel, G. Sapiro, Geodesic active contours, in: Processing of IEEE International Conference on Computer Vision'95, Boston, MA, 1995, pp. 694–699.

[4] V. Caselles, R. Kimmel, G. Sapiro, Geodesic active contours, International Journal of Computer Vision 22 (1) (1997) 61–79.

[5] T. Chan, L. Vese, Active contour without edges, IEEE Transaction on Image Processing 10 (2) (2001) 266–277.

[6] G.P. Zhu, Sh.Q. Zhang, Q.SH. Zeng, Ch.H. Wang, Boundary-based image segmentation using binary level set method, SPIE OE Letters 46 (5) (2007).

[7] J. Lie, M. Lysaker, X.C. Tai, A binary level set model and some application to Mumford–Shah image segmentation, IEEE Transaction on Image Processing 15 (2006) 1171–1181.

[8] D. Mumford, J. Shah, Optimal approximation by piecewise smooth function and associated variational problems, Communication on Pure and Applied Mathematics 42 (1989) 577–685.

[9] C.M. Li, C.Y. Xu, C.F. Gui, M.D. Fox, Level set evolution without re-initialization: a new variational formulation, in: IEEE Conference on Computer Vision and Pattern Recognition, San Diego, 2005, pp. 430–436.

[10] C.M. Li, C. Kao, J. Gore, Z. Ding, Implicit active contours driven by local binary fitting energy, in: IEEE Conference on Computer Vision and Pattern Recognition, 2007.

[11] C. Li, C. Kao, J. Gore, Z. Ding, Minimization of region-scalable fitting energy for image segmentation, IEEE Transactions on Image Processing 17 (2008) 1940–1949.

[12] Y. Shi, W.C. Karl, Real-time tracking using level sets, IEEE Conference on Computer Vision and Pattern Recognition 2 (2005) 34–41.

[13] P. Perona, J. Malik, Scale-space and edge detection using anisotropic diffusion, IEEE Transaction on Pattern Analysis and Machine Intelligence 12 (1990) 629–640.

[14] N. Paragios, R. Deriche, Geodesic active contours and level sets for detection and tracking of moving objects, IEEE Transaction on Pattern Analysis and Machine Intelligence 22 (2000) 1–15.

[15] S. Osher, R. Fedkiw, Level Set Methods and Dynamic Implicit Surfaces, Springer, New York, 2002.

[16] A. Tsai, A. Yezzi, A.S. Willsky, Curve evolution implementation of the Mumford–Shah functional for image segmentation, denoising, interpolation, and magnification, IEEE Transaction on Image Processing 10 (2001) 1169–1186.

[17] L.A. Vese, T.F. Chan, A multiphase level set framework for image segmentation using the Mumford–Shah model, International Journal of Computer Vision 50 (2002) 271–293.

[18] R. Ronfard, Region-based strategies for active contour models, International Journal of Computer Vision 46 (2002) 223–247.

[19] N. Paragios, R. Deriche, Geodesic active regions and level set methods for supervised texture segmentation, International Journal of Computer Vision 46 (2002) 223–247.

[20] R. Malladi, J.A. Sethian, B.C. Vemuri, Shape modeling with front propagation: a level set approach, IEEE Transaction on Pattern Analysis and Machine Intelligence 17 (1995) 158–175.

[21] H. Liu, Y. Chen, W. Chen, Neighborhood aided implicit active contours, IEEE Conference on Computer Vision and Pattern Recognition 1 (2006) 841–848.

[22] G. Aubert, P. Kornprobst, Mathematical Problems in Image Processing: Partial Differential Equations and the Calculus of Variations, Springer, New York, 2002.

[23] A. Vasilevskiy, K. Siddiqi, Flux-maximizing geometric flows, IEEE Transaction on Pattern Analysis and Machine Intelligence 24 (2002) 1565–1578.

[24] H.-K. Zhao, T. Chan, B. Merriman, S. Osher, A variational level set approach to multiphase motion, Journal of Computational Physics 127 (1996) 179–195.

About the Author—KAIHUA ZHANG was born in Rizhao, China, in 1983. He received his B.S. degree in science and technology of electronic information from Ocean University of China (OUC) in 2006 and master degree in signal and information processing from the University of Science and Technology of China (USTC) in 2009. Currently he is a research assistant in the department of computing, The Hong Kong Polytechnic University. His research interests include pattern recognition and image processing.

About the Author—HUIHUI SONG was born in Liao Cheng, China, in 1986. She received her B.S degree in science and technology of electronic information from Ocean University of China (OUC) in 2008. Currently she is a M.S. candidate of University of Science and Technology of China (USTC). Her research interests include pattern recognition and image processing.

About the Author—LEI ZHANG received the B.S. degree in 1995 from Shenyang Institute of Aeronautical Engineering, Shenyang, P.R. China, the M.S. and Ph.D degrees in Electrical and Engineering from Northwestern Polytechnical University, Xi'an, P.R. China, respectively, in 1998 and 2001. From 2001 to 2002, he was a research associate in the Department of Computing, The Hong Kong Polytechnic University. From January 2003 to January 2006 he worked as a Postdoctoral Fellow in the Department of Electrical and Computer Engineering, McMaster University, Canada. Since January 2006, he has been an Assistant Professor in the Department of Computing, The Hong Kong Polytechnic University. His research interests include image and video processing, biometrics, pattern recognition, computer vision, multisensor data fusion and optimal estimation theory, etc. Dr. Zhang is an associate editor of IEEE Transactions on Systems, Man and Cybernetics, Part C.